Influence of Yb doping on optical and upconversion photoluminescence properties of Yb-, Er-co-doped Y_2O_3 transparent ceramics prepared by SPS

Hiromi Kimura[1,*] , Takumi Kato[1], Shin-ichi Yamamoto[2], Daisuke Nakauchi[1], Noriaki Kawaguchi[1], and Takayuki Yanagida[1]

[1] Division of Materials Science, Nara Institute of Science and Technology (NAIST), 8916-5 Takayama-cho, Ikoma, Nara 630-0192, Japan

[2] Department of Electronics and Informatics, Faculty of Science and Technology, Ryukoku University, 1-5 Yokotani, Seta Oe-cho, Otsu, Shiga 520-2194, Japan

ABSTRACT

x% Yb-, 0.5% Er-co-doped Y_2O_3 transparent ceramics (x = 0, 0.1, 0.5, 1.0, 5.0 and 10) were prepared by the spark plasma sintering, and then we evaluated the effect of Yb doping on optical and upconversion (UC) photoluminescence (PL) properties. Under an excitation at 380 nm, the sharp emission peaks appeared around 550 and 660 nm, and the quantum yield was approximately 2%. The PL decay curves monitoring around 550 nm were fitted by a single exponential decay function. The decay time constants were 0.03–0.11 ms, and the values were typical for the 4f → 4f transitions of Er^{3+}. Regarding the UC PL properties, the sharp UC emission peaks around 550 and 660 nm were observed, and the UC emission intensity of 5.0% Yb-, 0.5% Er-co-doped Y_2O_3 transparent ceramic sample was the highest among the prepared samples. With increasing x, the chromaticity of UC emission color was tuned from green to red region. Regarding the UC PL decay curves, the rise time became slower as increasing x. This behavior is one of the evidence of energy transfer from Yb^{3+} to Er^{3+}.

1 Introduction

Phosphors are materials which exhibit a phenomenon of luminescence, and they have been used for a wide variety of devices such as white light-emitting diodes (LEDs) [1, 2], display devices [3, 4], solid-state lasers [5, 6] and radiation measurements [7, 8]. Among the phosphors, upconversion (UC) phosphors have a unique function to convert absorbed two or more low energy photons into high energy photon unlike conventional down-conversion luminescence. In particular, since UC phosphors can convert near-infrared radiation into visible light, they are expected to be applied in various applications including biomedical imaging [9–11], color displays [12, 13] and solar cells [14, 15].

Address correspondence to E-mail: kimura.hiromi.kf1@ms.naist.jp

Until now, almost all UC phosphors consist of host and dopant components. As the host components, there are many reports on oxide, fluoride and oxyfluoride materials such as Y_2O_3, $NaYF_4$ and LaOF [16–20]. In particular, Y_2O_3 has attracted much attention as host components of UC phosphors because of their good thermal and chemical properties and relatively low phonon energy (~ 380 cm^{-1}) [21, 22]. As the dopant components, trivalent lanthanide ions including Tb^{3+}, Ho^{3+}, Er^{3+}, Tm^{3+} and Yb^{3+} were often used. In particular, Er-, Yb-co-doped UC phosphors exhibited the intense UC emission because the Yb^{3+} ($^2F_{5/2} \to {}^2F_{7/2}$) emission and Er^{3+} ($^4I_{15/2} \to {}^4I_{11/2}$) absorption spectra were overlapped, which showed efficient energy transfer from Yb^{3+} to Er^{3+} [23–25].

In this study, we focus on Yb-, Er-co-doped Y_2O_3 for the above reasons. So far, almost all Yb-, Er-co-doped Y_2O_3 have been reported in the forms of nanoparticles [26, 27], film [28, 29], opaque ceramics [30, 31] and single crystal [32]. Recently, Y_2O_3 transparent ceramics were developed as new material forms and synthesized by the solid-state reaction [33], vacuum sintering [34], hot-isostatic pressing (HIP) [35] and spark plasma sintering (SPS) method [36]. Compared to single crystal, transparent ceramics have some advantages including lower sintering temperature, high mechanical strength and high uniformity of the dopant. However, when Y_2O_3 transparent ceramics were synthesized, the sintering aids such as La_2O_3 and ZrO_2 were generally used [37, 38]. Lu et al. and Guo et al. reported that the sintering aids affect UC properties [39, 40]. In contrast, Y_2O_3 transparent ceramics prepared by SPS can be obtained without any sintering aids [41]. Xiaorui et al. reported that Yb-, Er-co-doped Y_2O_3 transparent ceramics with various Er concentrations showed high UC emission [42]. However, there are no reports on Yb concentration dependence of UC PL properties in Yb-, Er-co-doped Y_2O_3 transparent ceramics synthesized by SPS.

The aim of this study is to investigate the effect of Yb doping on optical and UC PL properties of x% Yb-, 0.5% Er-co-doped Y_2O_3 transparent ceramics prepared by SPS (x = 0, 0.1, 0.5, 1.0, 5.0 and 10), and the optimal Yb concentrations are determined in terms of UC PL properties.

2 Experiment

x% Yb-, 0.5% Er-co-doped Y_2O_3 transparent ceramics with various concentrations of Yb (x = 0, 0.1, 0.5, 1.0, 5.0 and 10) were synthesized by the SPS machine (LabX-100, Sinter Land). As the raw powders, Y_2O_3 (> 99.99%, Furuuchi Chemical co., Ltd.), Er_2O_3 (> 99.99%, Furuuchi Chemical co., Ltd.) and Yb_2O_3 (> 99.99%, Nippon yttrium co., Ltd.) were used. The mixed powder was placed in a graphite die with two graphite punches and set into SPS machine. The SPS machine was operated as shown in Fig. 1. After the SPS sintering process, the samples were heated at 1200 °C for 8 h in the air atmosphere to remove oxygen vacancies. In the obtained samples, the surfaces were polished using a polishing machine (MetaServ 250, Buehler), and the thickness was fixed at 1.0 mm to evaluate optical and UC properties. For the phase identification, X-ray diffraction (XRD) patterns were obtained using X-ray diffractometer (MiniFlex, Rigaku). The density of samples was evaluated using the Archimedes method with pure water. As the optical properties, the in-line transmittance spectrum was obtained using a spectrometer (V670, JASCO). The photoluminescence (PL) excitation and emission spectra and quantum yield (QY) were measured by using Quantaurus-QY (C11347, Hamamatsu Photonics). The chromaticity of UC emission color was confirmed using a luminance colorimeter (BM-5A, Topcon) and plotted in the 1931 Commission International I'Eclairage (CIE) diagram. Under an excitation at 980 nm, UC PL spectra were obtained using original setup [43]. As the excitation source, we used a continuous-wave laser of 980 nm, and the laser power and power density were 200 mW and 11.3 W/

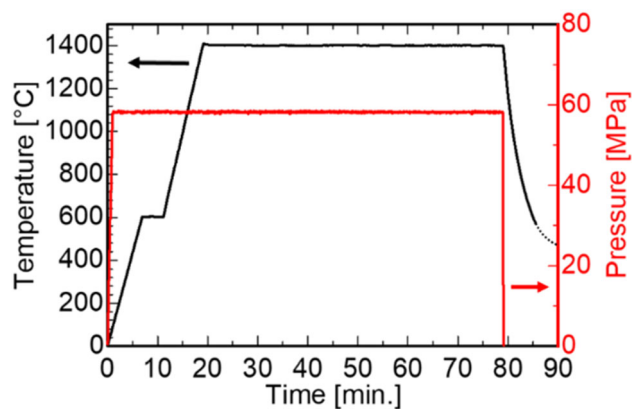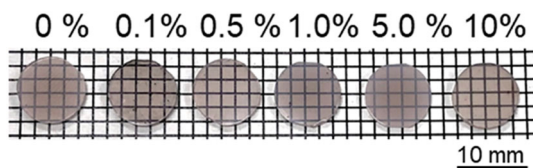**Fig. 1** SPS processing conditions

cm^2, respectively. To evaluate the decay time constant, PL decay curves were obtained using a Quantaurus-τ (C11367, Hamamatsu Photonics).

3 Results and discussion

3.1 Samples

Figure 2 shows a picture of polished Yb-, Er-co-doped Y$_2$O$_3$ transparent ceramic samples. All the samples showed transparency in the visible range, and the mesh patterns on the back of the samples could be seen. The samples look dark, which would be due to the carbon contamination from graphite die during the SPS processing. For the phase identification, the XRD patterns are presented in Fig. 3. All the diffraction peaks were in agreement with standard card patterns of cubic phase Y$_2$O$_3$ (COD: 1009014) without any additional peaks. Thus, all the samples were single phase. The peak positions were constant in all the sample because the ionic radius of Yb^{3+} (0.86 Å) was similar to that of Y^{3+} (0.89 Å). Therefore, Yb^{3+} ions can replace the Y^{3+} ions without significantly changing of the lattice parameter. The density and relative density of the samples are plotted in

Fig. 4. The density of $x = 0$ sample was 5.01 g/cm^3 which was close to the theoretical density of Y$_2$O$_3$ (5.013 g/cm^3) [44], and the relative density of all the samples was 99.7–99.9%. With increasing x, the density increased because the atomic mass of Yb was larger than that of Y.

3.2 Optical properties

Figure 5 represents in-line transmittance spectra of Yb-, Er-co-doped Y$_2$O$_3$ transparent ceramic samples. The transmittance of all the samples was $\sim$ 60% in the range of 1000 to 2700 nm. With the wavelength decreased, the transmittance was lowered. It may be attributed to some scattering centers including oxygen vacancies and grain boundary [45]. In fact, the behavior was similar to the previous studies about transmittance of Y$_2$O$_3$ transparent ceramics prepared by HIP and SPS [46–48]. In all the samples, some sharp absorption peaks due to the 4f $\rightarrow$ 4f transitions of Er^{3+} ions were observed [36, 49]. In addition, Yb-, Er-co-doped Y$_2$O$_3$ samples showed the absorption

Fig. 4 Density and relative density of Yb-, Er-co-doped Y$_2$O$_3$ transparent ceramic samples

Fig. 2 A picture of polished x% Yb-, 0.5% Er-co-doped Y$_2$O$_3$ transparent ceramic samples ($x = 0$, 0.1, 0.5, 1.0, 5.0 and 10)

Fig. 3 XRD patterns of Yb-, Er-co-doped Y$_2$O$_3$ transparent ceramic samples in the range of 10–90° (left) and 28–41°(right)

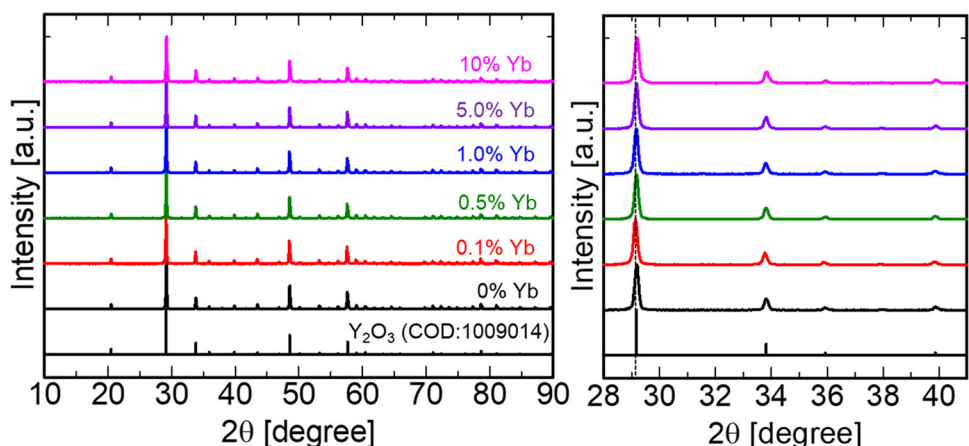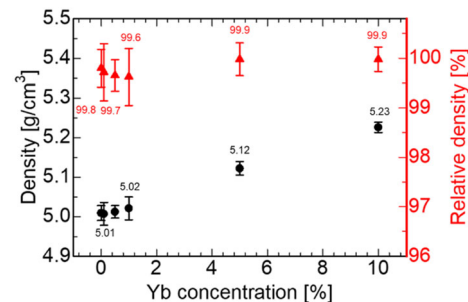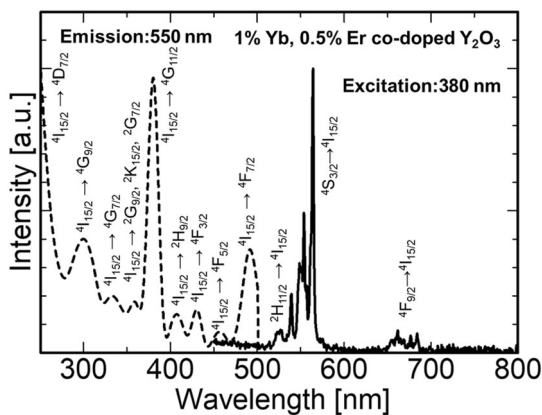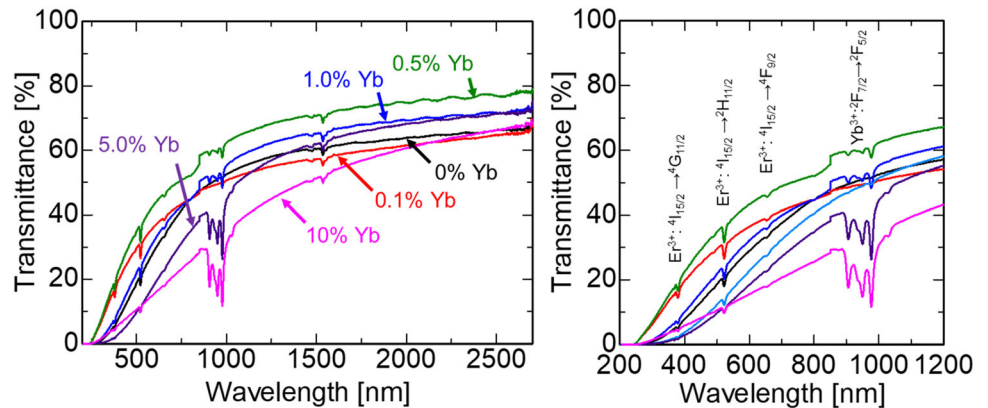**Fig. 5** In-line transmittance spectra of Yb-, Er-co-doped Y_2O_3 transparent ceramic samples in the range of 200 nm to 2700 nm (left) and 1200 nm (right)

Fig. 6 PL excitation (dotted line) and emission (solid line) spectra of 1.0% Yb-, 0.5% Er-co-doped Y_2O_3 transparent ceramic sample
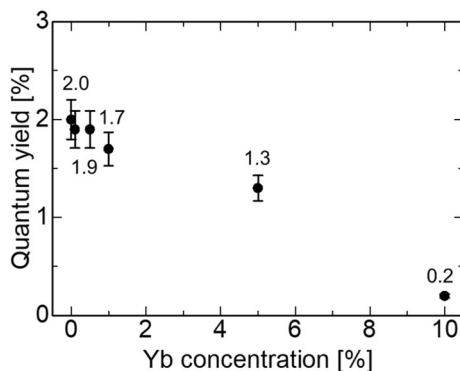
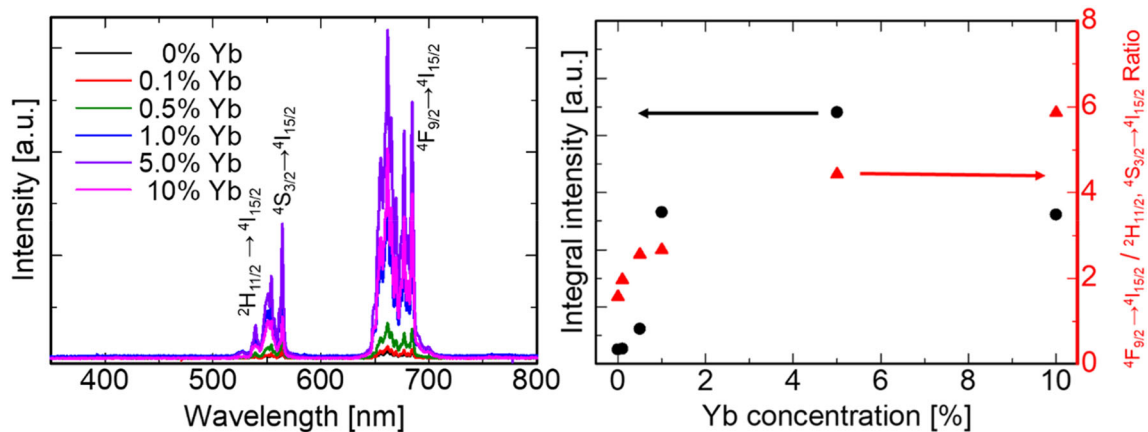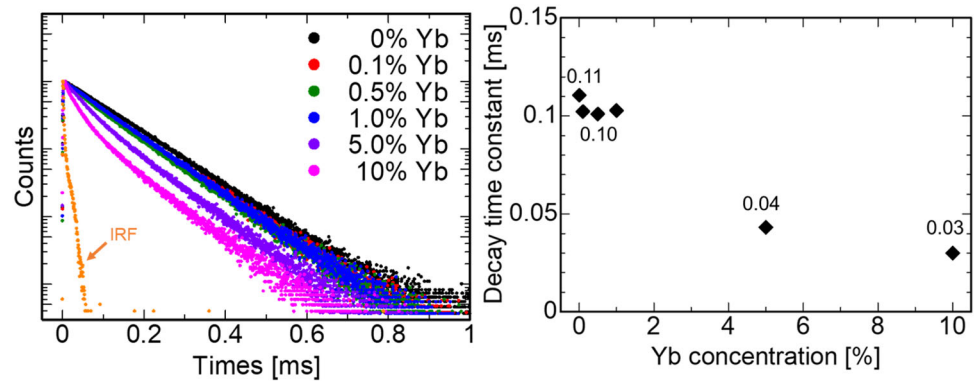**Fig. 7** PL QYs of Yb-, Er-co-doped Y_2O_3 transparent ceramic samples under an excitation at 380 nm

peaks around 950 nm ascribed to the 4f → 4f transitions of Yb^{3+} [35, 50, 51]. The intensity of absorption peaks due to Yb^{3+} increased with increasing x. Figure 6 shows PL excitation and emission spectra of 1.0% Yb-, 0.5% Er-co-doped Y_2O_3 transparent ceramic sample as a representative. The excitation and emission spectral shapes of all the samples were similar to that of 1.0% Yb-, 0.5% Er-co-doped sample. The multiple sharp excitation peaks appeared from 250 to 500 nm, which were typical for the 4f → 4f transitions of Er^{3+} ions. Under an excitation at 380 nm, the sharp emission peaks around 550 and 660 nm were observed. The emission peaks around 550 and 660 nm were assigned to the $^2H_{11/2}$, $^4S_{3/2}$ → $^4I_{15/2}$ and $^4F_{9/2}$ → $^4I_{15/2}$ transitions of Er^{3+} ions. The PL QYs of all the samples under an excitation at 380 nm are plotted in Fig. 7. The QYs of $x = 0$ sample was highest among the prepared samples. As the rise of x, the PL QYs decreased. Figure 8 represents PL decay curves of Yb-, Er-co-doped Y_2O_3 transparent ceramic sample monitoring around 550 nm under an excitation at 380 nm. To achieve an accurate evaluation, we deconvolute the IRF from the decay curves. All the curves were fitted by a single exponential decay function. The obtained decay time constants of all the samples were 0.03–0.11 ms, and the values were typical for the 4f → 4f transitions of Er^{3+} [52, 53]. When Yb concentrations increased, the decay time constants became faster. This trend was similar to the past report and it was related to the back energy transfer (BET) from Er^{3+} to Yb^{3+} ions [54].

3.3 Upconversion (UC) properties

Figure 9 shows UC PL spectra of Yb-, Er-co-doped Y_2O_3 transparent ceramic sample under an excitation at 980 nm. In all the samples, the sharp UC emission peaks around 550 and 660 nm were observed, and the origin of the peaks around 550 and 660 nm was due to the $^2H_{11/2}$, $^4S_{3/2}$ → $^4I_{15/2}$ and $^4F_{9/2}$ → $^4I_{15/2}$ transitions of Er^{3+} ions. The UC emission intensity of the $^2H_{11/2}$, $^4S_{3/2}$ → $^4I_{15/2}$ and $^4F_{9/2}$ → $^4I_{15/2}$ transitions of Er^{3+} ions increased with increasing x, and the

Fig. 8 PL decay curves (left) and decay time constants (right) of Yb-, Er-co-doped Y$_2$O$_3$ transparent ceramic sample monitoring around 550 nm under an excitation at 380 nm

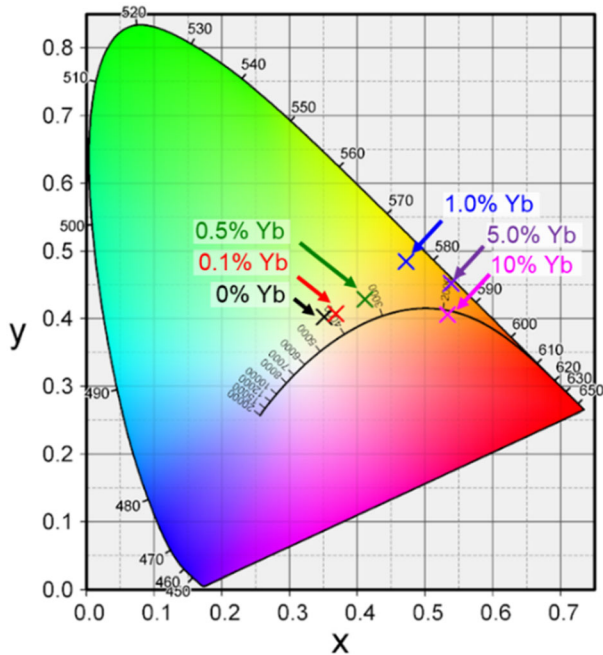**Fig. 9** UC PL spectra (left) and intensity (right) of Yb-, Er-co-doped Y$_2$O$_3$ transparent ceramic sample under an excitation at 980 nm

Fig. 10 Energy level diagram of Yb^{3+} and Er^{3+} ions and PL and UC emission mechanism
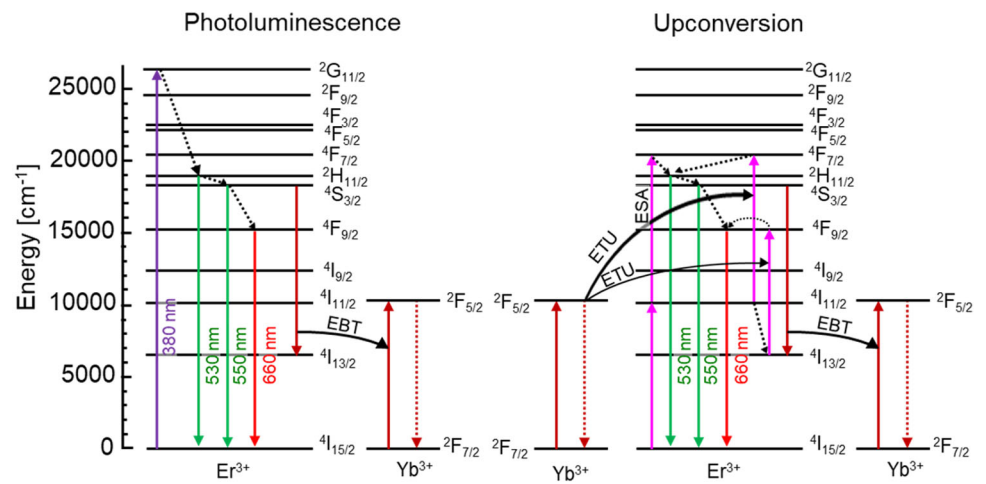
intensity of 5.0% Yb-, 0.5% Er-co-doped Y$_2$O$_3$ transparent ceramic sample was the highest among the prepared samples. According to the previous reports, the optimal Yb concentration of Yb-, Er-co-doped Y$_2$O$_3$ nanoparticles and ceramics was 8 and 2%,

respectively [55, 56]. Therefore, it is suggested that the optimal Yb concentration was different depending on the material forms. In addition, the UC PL intensity ratio ($^4F_{9/2} \rightarrow {}^4I_{15/2}$ / $^2H_{11/2}$, $^4S_{3/2} \rightarrow {}^4I_{15/2}$) gradually increased with increasing x unlike PL
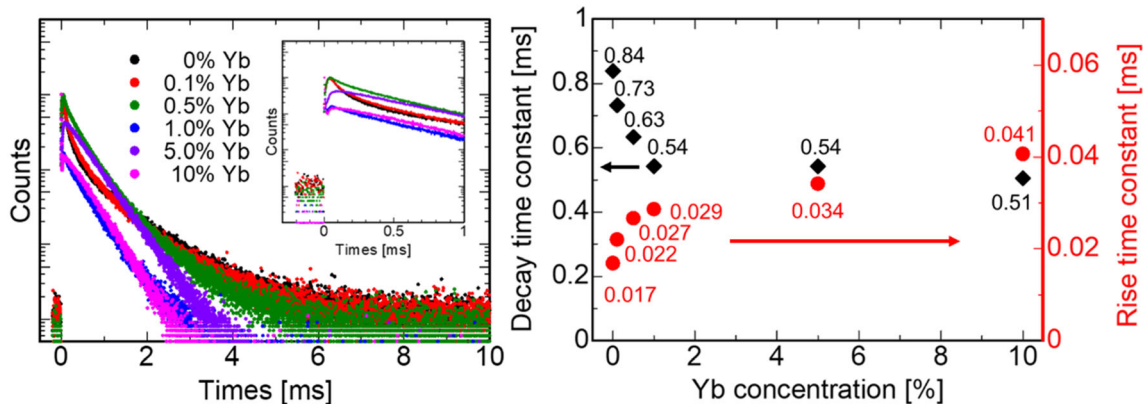
Fig. 11 Chromaticity coordinates of UC PL for Yb-, Er-co-doped Y_2O_3 transparent ceramic sample under an excitation at 980 nm

tions of Er^{3+} were ESA and ETU, respectively, because the absorption cross section of Yb^{3+} ions was much larger than that of Er^{3+} ions against an excitation of 980 nm [58]. Therefore, it was suggested that the process of (iii) increased as the increasing x, and UC emission ratio was changed.

Figure 11 shows chromaticity coordinates of UC PL for Yb-, Er-co-doped Y_2O_3 transparent ceramic sample under an excitation at 980 nm. The CIE color coordinates were located around green–yellow region in the $x = 0$ samples, and the color coordinates were shifted to yellow–red region with increasing x. This trend was confirmed in the past literature [22]. UC PL decay curves of Yb-, Er-co-doped Y_2O_3 transparent ceramic sample monitoring around 550 nm under an excitation at 980 nm are indicated in Fig. 12. The obtained UC PL decay curves under excitation at and 980 nm were fitted as $I(t) = I_0 \exp(-t/\tau_D) - I_1 \exp(-t/\tau_R)$, where I_0 and I_1 are positive constants, τ_D and τ_R are decay and rise time constants, respectively [15, 59]. The obtained decay and rise time constants were 0.51–0.84 and 0.017–0.041 ms, respectively. The decay and rise time constants of UC PL were slower in comparison with PL, and the rise time became slower as increasing x. Since the rise time constant was related to ETU process, it was suggested that the ETU process increased as the increasing x. In contrast, the decay time became faster with increasing x, and this tendency was observed in results of PL.

because there were differences in the luminescence mechanism between PL and UC emission as shown in Fig. 10. The UC luminescence mechanism of Yb-, Er-co-doped Y_2O_3 can be mainly classified into three different processes: (i) excited-state absorption (ESA), (ii) energy transfer upconversion (ETU) from Er^{3+} to Er^{3+} ions and (iii) ETU from Yb^{3+} to Er^{3+} ions [57]. In the Er-, Yb-co-doped Y_2O_3, the dominant processes of the $^2H_{11/2}$, $^4S_{3/2} \rightarrow ^4I_{15/2}$ and $^4F_{9/2} \rightarrow ^4I_{15/2}$ transi-

Fig. 12 UC PL decay curves (left) and decay and rise time constants (right) of Yb-, Er-co-doped Y_2O_3 transparent ceramic sample monitoring around 550 nm under an excitation at 980 nm

4 Conclusion

We have evaluated the effect of Yb doping on optical and UC PL properties of Yb-, Er-co-doped Y_2O_3 transparent ceramics synthesized by SPS. In $x = 0$ sample, the density was 5.01 g/cm^3 which was close to the theoretical density of Y_2O_3, and the relative density of all the samples was 99.7–99.9%. Regarding the PL and UC PL properties, the sharp emission peaks around 550 and 660 nm were observed under the excitation at 380 and 980 nm. Among the prepared samples, the UC emission intensity of 5.0% Yb-, 0.5% Er-co-doped Y_2O_3 transparent ceramic sample was the highest, and the chromaticity of UC emission color was shifted from green to red region with increasing x. When the monitoring wavelength was 550 nm, the decay time constants of PL and UC PL emission were 0.03–0.11 and 0.51–0.84 ms, which were the typical values for the $^2H_{11/2}$, $^4S_{3/2} \rightarrow ^4I_{15/2}$ transitions of Er^{3+}. Moreover, the rise time constant of UC PL emission became slower with increasing x. This behavior is one of the evidence of energy transfer from Yb^{3+} to Er^{3+}.

References

1. E.F. Schubert, Science **308**, 1274 (2005)
2. K. Bando, K. Sakano, Y. Noguchi, Y. Shimizu, J. Light Vis. Environ. **22**, 2 (1998)
3. D. Chen, W. Xiang, X. Liang, J. Zhong, H. Yu, M. Ding, H. Lu, Z. Ji, J. Eur. Ceram. Soc. **35**, 859 (2015)
4. K. Yoshimura, H. Fukunaga, M. Izumi, M. Masuda, T. Uemura, K. Takahashi, R.-J. Xie, N. Hirosaki, J. Soc. Inf. Disp. **24**, 449 (2016)
5. T. Sanamyan, Laser Phys. Lett. **12**, 125804 (2015)
6. J. Lu, J. Lu, T. Murai, K. Takaichi, T. Uematsu, K. Ueda, H. Yagi, T. Yanagitani, A.A. Kaminskii, Jpn. J. Appl. Phys. **40**, L1277 (2001)
7. C.W.E. van Eijk, Nucl. Instruments Methods Phys. Res. A **460**, 1 (2001)
8. H. Kimura, T. Kato, D. Nakauchi, G. Okada, N. Kawaguchi, T. Yanagida, Nucl. Instruments Methods Phys. Res. A **954**, 161226 (2020)
9. L. Wang, M.S. Draz, W. Wang, G. Liao, Y. Xu, J. Biomed. Nanotechnol. **11**, 325 (2015)
10. G. Kaur, S.B. Rai, Luminescence **28**, 143 (2013)
11. C. Duan, L. Liang, L. Li, R. Zhang, Z.P. Xu, J. Mater. Chem. B **6**, 192 (2018)
12. B. Zhu, B. Qian, Y. Liu, C. Xu, C. Liu, Q. Chen, J. Zhou, X. Liu, J. Qiu, NPG Asia Mater. **9**, e394 (2017)
13. L. Gao, X. Shan, X. Xu, Y. Liu, B. Liu, S. Li, S. Wen, C. Ma, D. Jin, F. Wang, Nanoscale **12**, 18595 (2020)
14. X. Huang, S. Han, W. Huang, X. Liu, Chem. Soc. Rev. **42**, 173 (2013)
15. X. Chen, W. Xu, H. Song, C. Chen, H. Xia, Y. Zhu, D. Zhou, S. Cui, Q. Dai, J. Zhang, A.C.S. Appl, Mater. Interfaces **8**, 9071 (2016)
16. Y. Zhang, L. Zhang, R. Deng, J. Tian, Y. Zong, D. Jin, X. Liu, J. Am. Chem. Soc. **136**, 4893 (2014)
17. Q. Zhao, J. Zhao, M. Tao, C. Wang, X. Zeng, Y. Hu, S. Wang, M. Zeng, W. Zhou, Y. Li, J. Lumin. **214**, 116580 (2019)
18. E. Palo, L. Pihlgren, M. Tuomisto, T. Laihinen, I. Hyppänen, J. Kankare, M. Lastusaari, T. Soukka, H.C. Swart, J. Hölsä, Opt. Mater. **59**, 49 (2016)
19. G.Y. Chen, H.C. Liu, G. Somesfalean, Y.Q. Sheng, H.J. Liang, Z.G. Zhang, Q. Sun, F.P. Wang, Appl. Phys. Lett. **92**, 113114 (2008)
20. S.-I. Yamamoto, K. Ohyama, T. Ban, T. Nonaka, Mater. Res. Express **6**, 036202 (2018)
21. A. Ubaldini, M.M. Carnasciali, J. Alloys Compd. **454**, 374 (2008)
22. L.A. Diaz-Torres, P. Salas, J. Oliva, E. Resendiz-L, C. Rodriguez-Gonzalez, O. Meza, Appl. Phys. A **123**, 25 (2017)
23. J. Zhang, Z. Hao, J. Li, X. Zhang, Y. Luo, G. Pan, Light Sci. Appl. **4**, e239 (2015)
24. T. Nonaka, T. Ban, S.-I. Yamamoto, Trans. Mater. Res. Soc. Jpn. **42**, 139 (2017)
25. B.-C. Hwang, S. Jiang, T. Luo, J. Watson, G. Sorbello, N. Peyghambarian, J. Opt. Soc. Am. B **17**, 833 (2000)
26. R. Tomala, W. Strek, Opt. Mater. **109**, 110047 (2020)
27. Y. Li, Y. Zhang, G. Hong, Y. Yu, J. Rare Earths **26**, 450 (2008)
28. G. Cabello-Guzmán, D. González, C. Caro-Díaz, L. Lillo-Arroyo, F. Valenzuela-Melgarejo, G. Cárdenas Triviño, G.E. Buono-Core, B. Chornik, Y. Huentupil, J. Lumin. **204**, 401 (2018)
29. B. Xu, J. Liu, K. Zou, Appl. Phys. A **125**, 100 (2019)

30. V. Singh, P. Haritha, V. Venkatramu, S.H. Kim, Spectrochim. Acta A **126**, 306 (2014)

31. R. Dey, A. Pandey, V.K. Rai, Sens. Actuators B **190**, 512 (2014)

32. R. Bao, N. An, L. Ye, L.-G. Wang, Opt. Fiber Technol. **52**, 101989 (2019)

33. N. Wang, X. Zhang, H. Jiang, T. Dong, D. Yang, Mater. Chem. Phys. **135**, 709 (2012)

34. G. Zhao, Q. Yang, Q. Liu, S. Lu, J. Alloys Compd. **583**, 372 (2014)

35. J. Wang, J. Ma, J. Zhang, P. Liu, D. Luo, D. Yin, D. Tang, L.B. Kong, Opt. Mater. **71**, 117 (2017)

36. J. Zhang, S. Wang, L. An, M. Liu, L. Chen, J. Lumin. **122–123**, 8 (2007)

37. Q. Yi, S. Zhou, H. Teng, H. Lin, X. Hou, T. Jia, J. Eur. Ceram. Soc. **32**, 381 (2012)

38. K. Ning, J. Wang, J. Ma, Z. Dong, L.B. Kong, D. Tang, Mater. Today Commun. **24**, 101185 (2020)

39. S. Lu, Q. Yang, B. Zhang, H. Zhang, Opt. Mater. **33**, 746 (2011)

40. Y. Guo, X. Wu, Q. Wang, D. Wang, Mater. Sci. Pol. **38**, 159 (2020)

41. H. Furuse, S. Nakasawa, H. Yoshida, K. Morita, T.S. Suzuki, B.-N. Kim, Y. Sakka, K. Hiraga, J. Am. Ceram. Soc. **101**, 694 (2018)

42. X. Hou, S. Zhou, W. Li, Y. Li, H. Lin, H. Teng, T. Jia, J. Am. Ceram. Soc. **93**, 2779 (2010)

43. T. Nonaka, T. Kanamori, K. Ohyama, S.I. Yamamoto, Jpn. J. Appl. Phys. **54**, 03CA02 (2015)

44. A. Camenzind, R. Strobel, S.E. Pratsinis, Chem. Phys. Lett. **415**, 193 (2005)

45. W. Zhang, T. Lu, N. Wei, Y. Wang, B. Ma, F. Li, Z. Lu, J. Qi, J. Alloys Compd. **520**, 36 (2012)

46. W.K. Jung, H.J. Ma, Y. Park, D.K. Kim, Scr. Mater. **137**, 1 (2017)

47. X. Huang, X. Zhang, Z. Hu, Y. Feng, J. Wei, X. Liu, X. Li, H. Chen, L. Wu, H. Pan, J. Li, Opt. Mater. **92**, 359 (2019)

48. Z. Hu, X. Xu, J. Wang, P. Liu, D. Li, X. Wang, J. Zhang, J. Xu, D. Tang, J. Eur. Ceram. Soc. **38**, 1981 (2018)

49. J. Zhou, Y. Chen, R. Lei, H. Wang, S. Xu, J. Lumin. **215**, 116671 (2019)

50. L. Zhang, W. Pan, J. Feng, J. Eur. Ceram. Soc. **35**, 2547 (2015)

51. J. Zhang, L. An, M. Liu, S. Shimai, S. Wang, J. Eur. Ceram. Soc. **29**, 305 (2009)

52. A.N. Meza-Rocha, E.F. Huerta, U. Caldiño, E. Zaleta-Alejandre, S.H. Murrieta, J.M. Hernández, E. Camarillo, Z. Rivera-Álvarez, G.C. Righini, C. Falcony, J. Lumin. **154**, 106 (2014)

53. M. Sun, J. Liu, L. Nie, J. Alloys Compd. **816**, 152575 (2020)

54. V.K. Tikhomirov, V.D. Rodríguez, J. Méndez-Ramos, J. Del-Castillo, D. Kirilenko, G. Van Tendeloo, V.V. Moshchalkov, Sol. Energy Mater. Sol. Cells **100**, 209 (2012)

55. Y. Tian, Y. Fu, M. Xing, X. Luo, J. Nanomater. **2015**, 1 (2015)

56. H. Wang, C. Duan, P.A. Tanner, J. Phys. Chem. C **112**, 16651 (2008)

57. D. Matsuura, Appl. Phys. Lett. **81**, 4526 (2002)

58. J. Liao, L. Nie, S. Liu, B. Liu, H. Wen, J. Mater. Sci. **49**, 6081 (2014)

59. R. Martín-Rodríguez, S. Fischer, A. Ivaturi, B. Froehlich, K.W. Krämer, J.C. Goldschmidt, B.S. Richards, A. Meijerink, Chem. Mater. **25**, 1912 (2013)